Electronic Supplementary Material (ESI) for Journal of Materials Chemistry C.

Supplementary Information

Mechanical-tuning of the cooperativity of spin-crossover particles via the matrix crystallization and related size effects

J. Laisney,[a‡] D. Morineau,[b,*] C. Enachescu,[c,*] R. Tanasa,[c] E. Rivière,[a] R. Guillot,[a] M.-L. Boillot[a,*]
[a] Institut de Chimie Moléculaire et des Matériaux d'Orsay, Univ. Paris-Sud 11, Université Paris-Saclay, CNRS, 91405 Orsay, France
[b] University of Rennes 1, Institut de Physique de Rennes, UMR UR1-CNRS 6251, 35000 Rennes, France.
[c] Faculty of Physics, Alexandru Ioan Cuza University, 700506 Iasi, Romania.
‡Present address, Dept of Plant and Soil Sciences, University of Kentucky, Lexington, Kentucky, 40546, USA.

Content

Experimental details

Syntheses of Fe^{III}(3-OMeSalEen)$_2$]PF$_6$

Polycrystalline powder and single-crystals. The complex was prepared as previously reported.[1] Elemental analysis (%) Calcd (Found) for $C_{26}H_{40}F_6FeN_4O_4P$: C, 44.80 (44.58); H, 5.33 (5.38); N, 8.71 (8.55). The RT powder X-ray diffractogram was found to be consistent with that simulated from the 300 K single-crystal X-ray structure. Optical microscope images of the powder show crystals with a 50 - 200 µm size.

Nano- and microcrystals. The synthesis[2] was done at -60°C using an antisolvent (butanol, 20 mL) and a solvent (acetone, 1 mL) afforded 460(140)x200(50)x35(10) nm^3 sized platelets as determined from TEM measurements. The microcrystals prepared at +40 °C (0.5 mL of acetonitrile as solvent) correspond to the expectation (8(4)x0.7(0.3)x0.15(0.07) µm^3).

---

[1] A. Tissot et al *J. Mater. Chem.* **2011**, 21, 18347.

[2] A. Tissot et al *J. Mater. Chem.* **2012**, 22, 3411.

TEM measurements. The TEM images were acquired on a TEM JEOL 1400 (120 kV) equipped two high-resolution and high-speed digital CCD Gatan camera.

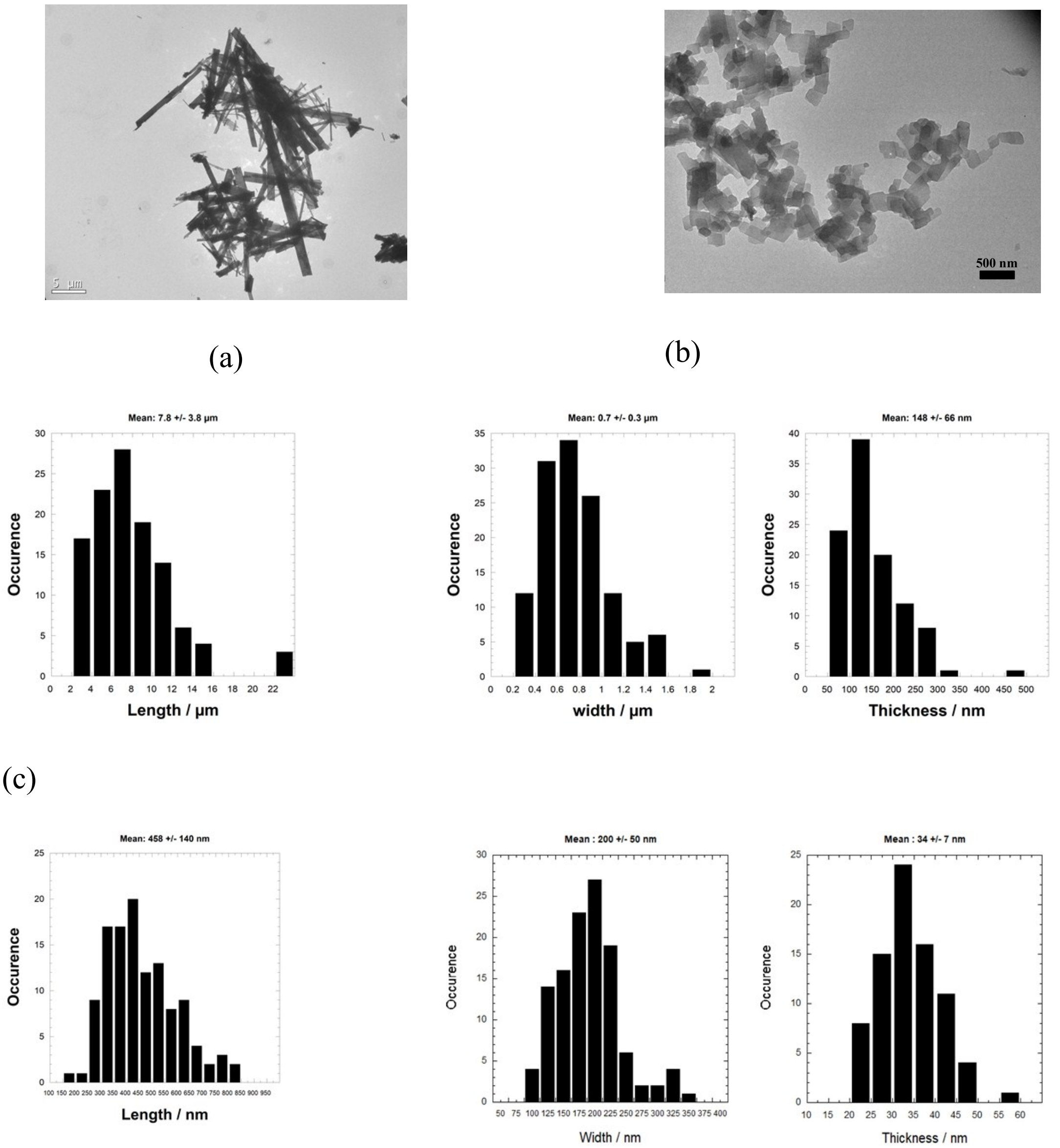

(a)

(b)

(c)

(d)

Fig. S1: TEM images of the Fe^{III}(3-MeO-SalEen)$_2$]PF$_6$ microparticles (a, c) and nanoparticles (b, d) together with the corresponding size distribution curves determined by TEM measurements.

Matrix effects. They were studied from the coating (single crystals) or dispersions (34 wt-% of polycrystals, 26 wt-% of micro- or 33 wt-% of nanocrystals) in 1-Butanol *(*purchased from Alfa-Aesar, 99 %). FORCs investigations were achieved with 2-3 wt-% (Iasi's Lab) and 32wt-% (Orsay's Lab) dispersion of powder in BuOH. The determination of the unit-cell parameters of single crystals was achieved with 1-butanol and Paratone, also named Parabare 10312 (Hampton Research), that is used as cryoprotectant for crystallography.[3]

Calorimetric measurements. The differential scanning calorimetry (DSC) measurements were performed with a Q-20 TA Instrument equipped with a liquid nitrogen cooling system. The melting transition of an indium sample was used for calibration of temperature and heat flux. The samples were loaded in aluminium hermetic pans.

Two modes were used: (i) a classical DSC mode, where the temperature was ramped linearly (scanning rate of 10 $\mathrm{Kmin^{-1}}$), (ii) a modulated m-DSC mode, where a slight sinusoidal modulation of the temperature (period 40s, amplitude ΔT = +/- 0.1K) was added to a slower linear ramp (scanning rate of 1 $\mathrm{K.min^{-1}}$). These conditions ensure a good control of the thermal stationary equilibrium of the samples, while monitoring the DC and AC component of the heat flux. The set of parameters used fulfils the 'heat-only/cool-only' condition, meaning that the temperature variation is always monotonous, despite the sinusoidal modulation.

---

[3] Plonka et al *Angew. Chem. Int. Ed.* **2013**, 52, 1692 ; I. Stanciu *Orient. J. Chem.* **2015**, 31, 1383).

).

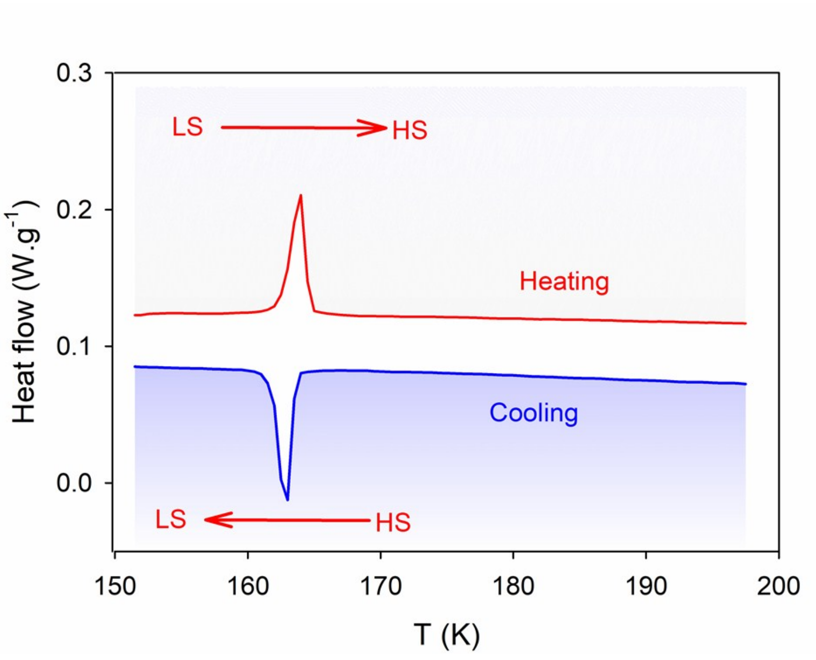

Fig. S2: Total heat flow of the m-DSC thermogram (scanning rate = 1 K.min^{-1}) of free SC polycrystals (bulk) cycled in the temperature range 150-200K.

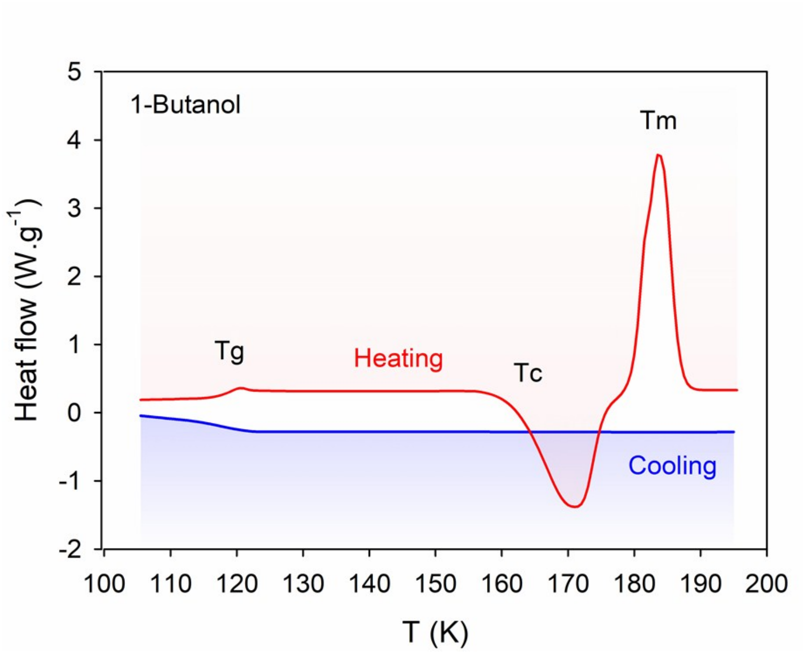

Fig. S3: Thermogram of 1-butanol at 10 K.min^{-1} cycled in the range from 100 to 200 K. 1-butanol was supercooled on cooling and formed a glass. On heating, above the glass transition (T_g = 118K) it crystallized (above T_c = 160 K) and melted (T_m = 183.7 K, ΔH = 96 J.g^{-1}).

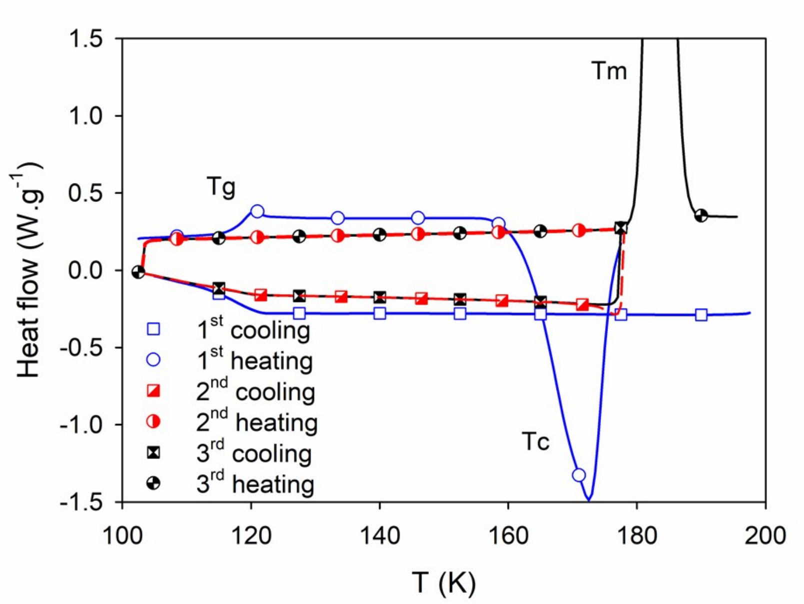

Fig. S4: Thermogram of 1-butanol at 10 K.min^{-1} cycled in the range from 100 to 200 K. After cooling down from 200K to 100 K deep in the glass, the first heating branch was interrupted at 180K (i.e. after cold crystallization was induced above Tc, but before melting at Tm), and two thermal cycles in the range 100-180 K were performed. It revealed that the crystallization was complete (absence of any signs of the glass transition or crystallisation), but a same endothermic peak as in Fig. S3 due to the melting during the final heating up to 200K.

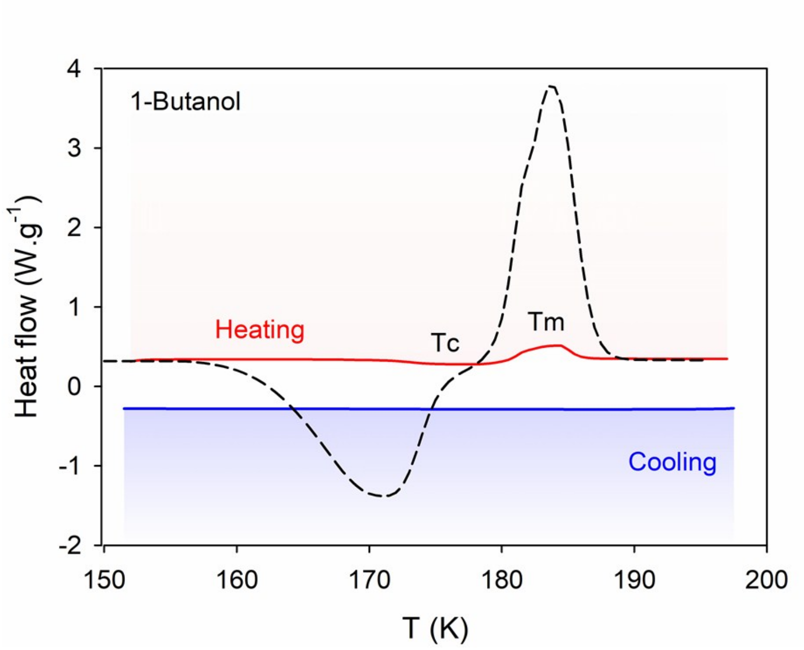

Fig. S5: Thermogram of 1-butanol at 10 K.min^{-1} cycled in the range from 150 to 200 K. On heating, BuOH remains liquid in a range of temperature overlapping that of SCO. The exothermic and endothermic peaks ($\Delta H = 3.5$ J.g^{-1}) indicate that crystallization concerns only a small fraction of 1-butanol (c.a. 4%) and is shifted to above 170 K. This behaviour contrasts with the full crystallization observed when the cycled temperature range was from 100 to 200 K, as shown in Fig. S3, and recalled in dashed line for comparison.

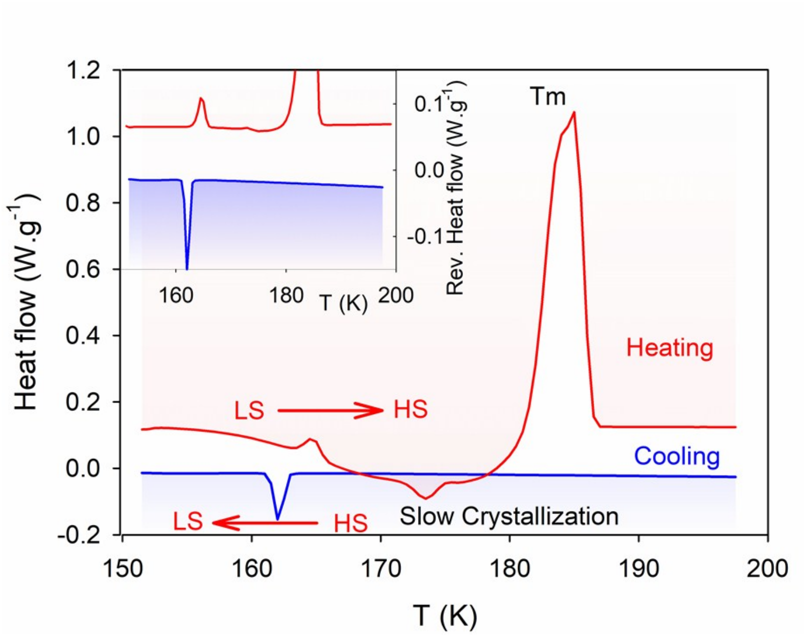

Fig. S6: Total heat flow of the m-DSC thermogram (1 K.min^{-1}) of SC polycrystals (33 wt-%) embedded in BuOH cycled in the temperature range 150-200 K. The SC transitions occurs in the liquid matrix, despite the initiation of crystallization on heating, the latter contribution being absent in the reversing heat flow (inset).

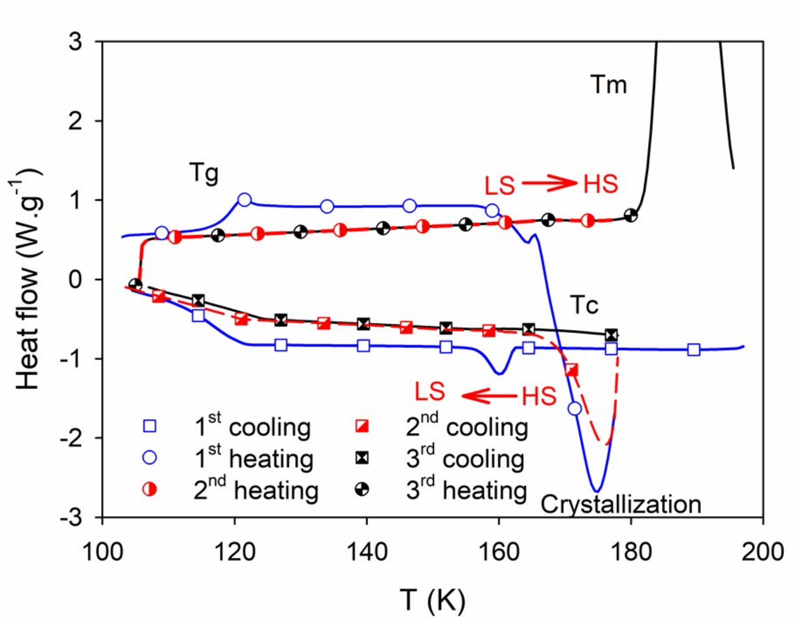

Fig. S7: Thermogram of microcrystals embedded in 1-butanol at 10 K.min^{-1} cycled in the range from 100 to 200 K, following the same protocol as for pure 1-butanol presented in Fig. S4. After cooling down from 200K to 100 K deep in the glass, the first heating branch was interrupted at 180K (cycle #1), which induced matrix crystallization. Two thermal cycles in the range 100-180 K (cycle #2,3) were performed in the crystal, and melting was achieved during the final heating up to 200K. The SC transitions observed during cycle #1 occurred in a liquid matrix, while in subsequent cycles (#2,3), the SC process took place in a fully crystallized matrix.

Tab. S1: Thermal characteristics of phase transitions of Fe^{III}(3-OMeSalEen)$_2$]PF$_6$ in the form of free or embedded particles (polycrystals, 8 µm-long microcrystals). The data were extracted from DSC thermograms collected at 10 Kmin^{-1}.

	Polycrystals				**Microcrystals**			
Cooling/heating cycle	Temperature (K)				Temperature (K)			
[T range] Cycle label (n)	$T_{max}\downarrow$	$T_{max}\uparrow$	$T_{1/2}$	ΔT	$T_{max}\downarrow$	$T_{max}\uparrow$	$T_{1/2}$	ΔT
	Free particles				Free particles			
[200-100-200K]	162.0	164.5	163.2	2.5	161.6	164.4	163.0	2.8
	In-BuOH particles				In-BuOH particles			
[200-150-200K]	161.9	164.6	163.2	2.7	160.0	165.6	162.8	5.6
[200-100-200K](0)	162.1	*164.3*	*163.0*	*2.2*	160.2	*164.8*	*162.5*	*4.6*
[200-100-180K](1)	162.0	*164.4*	*163.0*	*2.4*	160.1	*164.*9	*162.5*	*4.8*
[180-100-180K](2)	156.1	164.2	160.1	8.0	*152.4*	164.7$^{(*)}$	-	-
[180-100-200K](3)	158.2	164.2	161.2	6.0	151.6$^{(*)}$	164.6$^{(*)}$	-	-

$T_{1/2}$= (T↑+ T↓)/2; ΔT= T↑− T↓ ; Cycle label (n) as defined in Fig. S7. In italic, convoluted peak due to the crystallization of 1-butanol; (*) residual peak.

Compared to the polycrystals, the sample of microcrystals is characterized by a slightly reduced size, a specific needle-type shape and more controlled related distributions. The dispersion of particles in the liquid keeps unchanged the $T_{1/2}$ value and shifts the position of maxima by 1-2 K. In comparison to the pure sample, the shape of the transition peaks is less asymmetric but broadened. Because of the scanning rate of 10 Kmin^{-1}, the formation of the glacial phase of BuOH is prevented and here we can observe how the crystallization of triclinic phase influences the process of spin transition. The LS-to-HS signal is detectable but essentially convoluted with that of BuOH. Further cooling or heating cycles result in a net decrease of intensity (by a factor ~ 6), the broadening and the shift (a several K downshift of the HS-to-LS branch) of SC peaks. So, upon the thermal cycling in 1-butanol, similar evolutions characterize the polycrystals and microcrystals samples.

Magnetic measurements. The data were collected at a scanning rate of 4, 1 or 0.5 Kmin^{-1} with an iterative regression algorithm and a magnetic field of 5000 Oe. The samples (34wt-% of SC polycrystalline powder dispersed in BuOH) were thermally cycled according to the conditions defined for the calorimetric measurements.

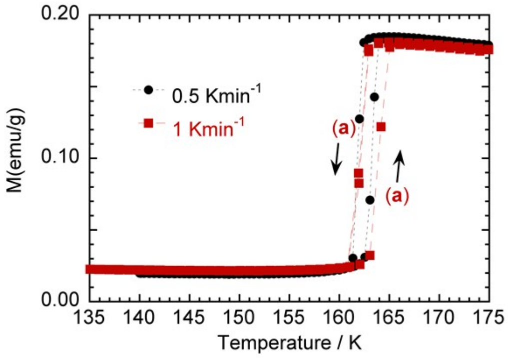

Fig. S8: Magnetization *vs.* Temperature plots of [Fe^{III}(3-OMeSalEen)$_2$]PF$_6$ in the form of a polycrystalline powder (scanning rate = 1, 0.5 Kmin^{-1}).

In Figures S9-S11, the label (**a**, **b**, **c** or **d**) of the observed cycles refers to the Table 2 in the main text.

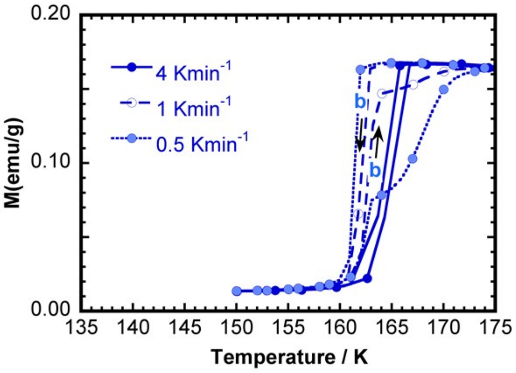

Fig. S9: Magnetization vs. temperature plots of the polycrystalline particles (bulk) embedded in liquid butanol (**b**). After thermalization at 200 K (30 min), the sample was thermally cycled between 180 and 150 K (scanning rate = 4, 1 and 0.5 Kmin^{-1}).

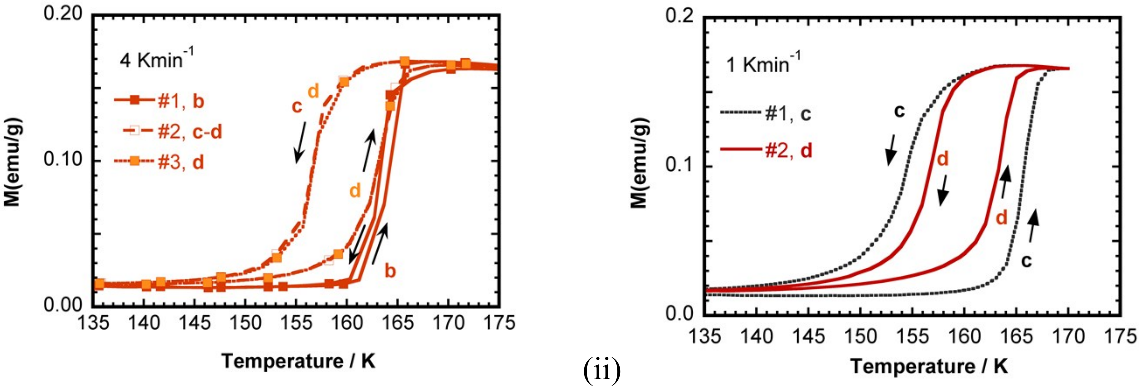

(i) (ii)

Fig. S10: Magnetization vs. temperature plots of the polycrystals embedded in 1-butanol. In (i): after the thermalization (200 K, 30 min): three successive full cycles (# n, n = 1-3) performed at 4 Kmin^{-1} in which the butanol is liquid (#1, 200-100 K, **b**) then crystalline (#2, 180-100 K, **c-d**; #3, 180-100 K, **d).** In (ii), after the thermalization (90 K, 2 h), two successive cycles (#1, 90-170 K, **c**) and (#2, 90-170 K, **d**) performed at 1 Kmin^{-1}.

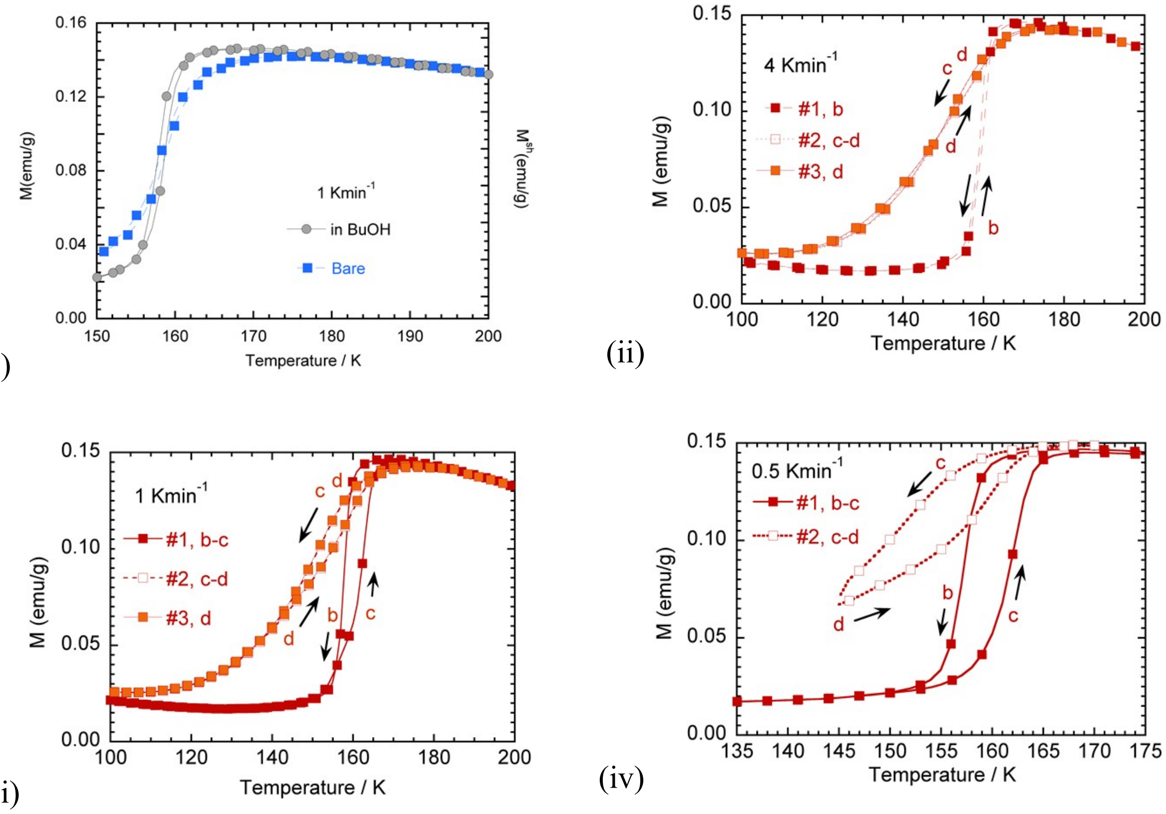

(i) (ii) (iii) (iv)

Fig. S11: Magnetization vs Temperature plots of the nanoparticles embedded in butanol performed at different scanning rates after a 200 K thermalization (30 min): (i) the 200 - 150 K cycle (**b)** superposed with that of bare particles (**a**) performed at 1 Kmn^{-1}; (ii) the 200 – 100 - 180 K cycle (■, #1, **b**) then two successive 180 - 100 - 180 K cycles (⊙, #2, **c-d)** and (■,#3, **d**) performed at 4 Kmin^{-1}; (iii) same cycle as in (ii) performed at 1 Kmin^{-1}; (iv) superposition of the 180-100 K cycle (■, #1, **b-c**) followed by a stabilization at 145 K (30 min) then the full 170-145 K cycle (⊙, #2, **c-d)** performed at 1Kmin^{-1}.

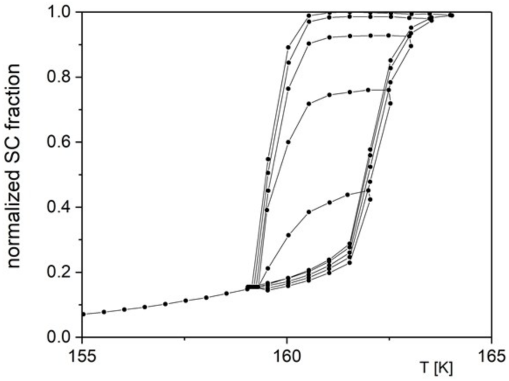

Fig. S12: Hysteresis of microparticles and related FORCs in the cooling mode (**d**).

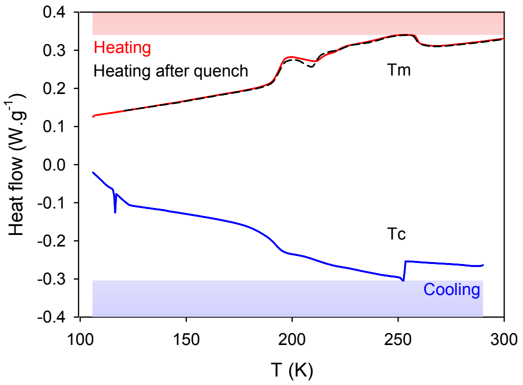

Fig. S13: DSC thermogram of Paratone (or Parabare 10312, Hampton Research) between 300 and 100 K (10 Kmin^{-1}). Paratone is a multicomponent blend that solidifies between 260 and 190 K. [4,5]

---

[4] Plonka et al *Angew. Chem. Int. Ed.* **2013**, 52, 1692.
[5] I. Stanciu *Orient. J. Chem***. 2015**, 31, 1383.

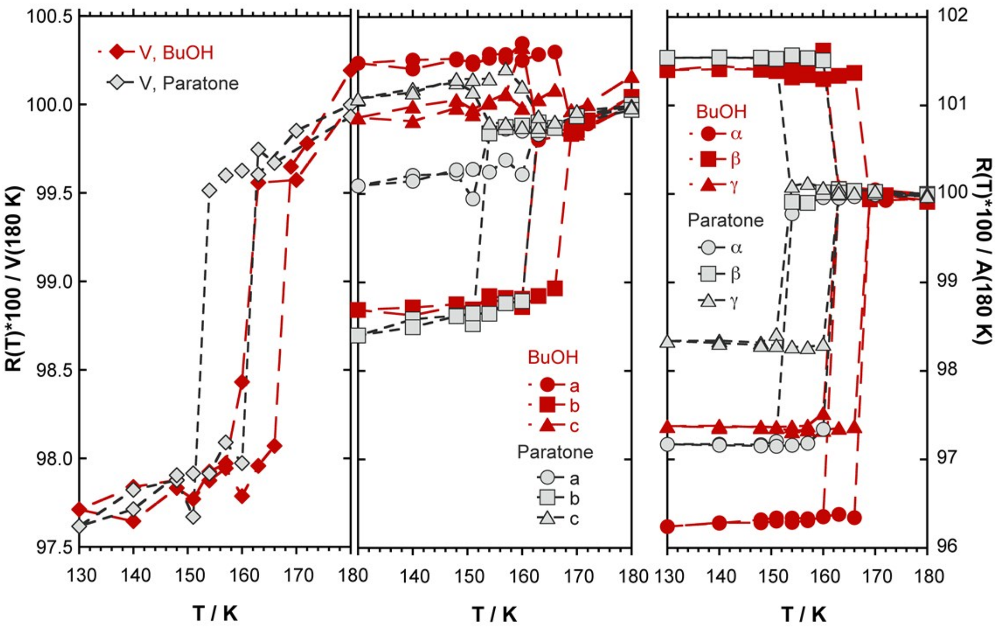

Fig. S14: (a) Relative evolution of the unit-cell parameters (noted R) as a function of temperature: (a) the volume lattice, (b) the a (●), b (■), c (□) axes, and (c) the α (●), β (■), γ (□) angles in the case of single crystals coated with BuOH (full symbol in red) and Paratone (full symbol in grey).

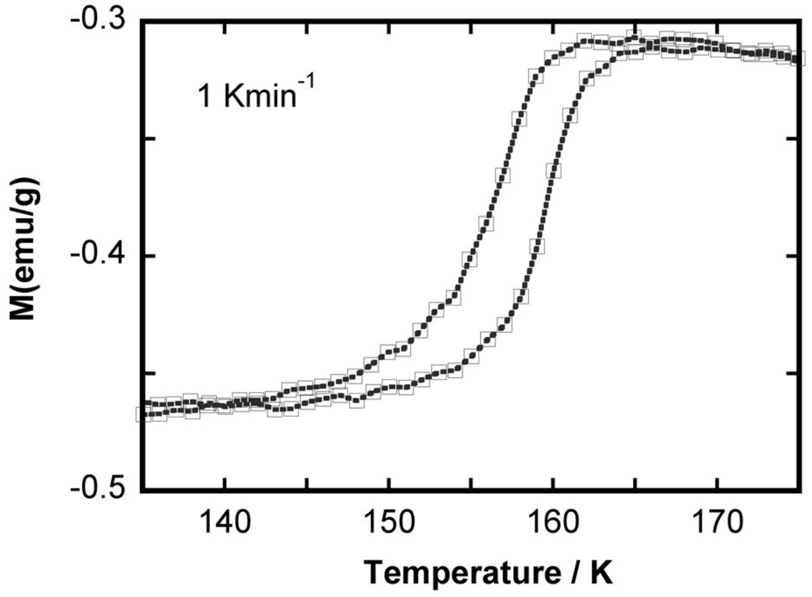

Fig. S15: Magnetization vs. temperature plots for a powder of polycrystals embedded in Paratone (1 Kmin^{-1}).

Compared to the pure sample ($T_{1/2}$ = = 161 K, $\Delta T \leq 1$ K), the sample dispersion in Paratone results in a relatively smoother transition curve that is centered at a lower temperature and a hysteresis loop which slightly varies upon the thermal cycling as a consequence of the environment-particle relaxation ($T_{1/2}$ = 156-158 K, ΔT = 5 then 3 K).